

Tracing the structure of the Milky Way with detached eclipsing binaries from the VVV survey — I. The method and initial results.*

K. G. Helminiak^{1,2†}, J. Devor³, D. Minniti^{1,4,5} and P. Sybilski²

¹*Departamento de Astronomía y Astrofísica, Facultad de Física, Pontificia Universidad Católica de Chile, Av. Vicuña Mackenna 4860, 782-0436 Macul, Santiago, Chile*

²*Nicolaus Copernicus Astronomical Center, Department of Astrophysics, ul. Rabiańska 8, 87-100 Toruń, Poland*

³*School of Physics and Astronomy, Tel Aviv University, Tel Aviv 69978, Israel*

⁴*Vatican Observatory, V-00120 Vatican City State, Italy*

⁵*Departamento de Ciencias Físicas, Universidad Andres Bello, Santiago, Chile*

Accepted Received; in original form ...

ABSTRACT

We present the first results of a project aiming to trace the spatial structure of the Milky Way using detached eclipsing binaries (DEBs) as distance indicators. A sample of DEBs from the OGLE-II catalogue was selected and their near infrared photometry was taken from the Vista Variables in the Via Lactea (VVV) survey. The I band OGLE-II light curves are used to create models of the DEBs, which together with the VVV photometry are compared with a set of theoretical isochrones. After correcting for stellar reddening, we find a set of absolute physical parameters of components of a given binary, including absolute magnitudes and distances.

With this approach we can calculate the distances with the precision better than 5 per cent. Even though we have a few systems, the distribution is not homogeneous along the line of sight, and appears to follow the overall structure of the Galaxy – several spiral arms and the Bulge are distinguishable. A number of systems can be seen behind the Bulge, reaching even the distance to the Sagittarius dwarf galaxy.

Key words: Galaxy: structure – binaries: eclipsing.

1 INTRODUCTION

Detached eclipsing binaries (DEBs) are extremely powerful tools in astronomical research. They allow us to derive a complete set of physical parameters of stars, including their absolute magnitudes. Having them, one can calculate the distance, or at least the distance modulus, by comparing the derived absolute magnitudes from the model with the observed ones. This however normally requires spectroscopic observations to calculate radial velocities of both components. They are used for calculating the masses and orbital parameters, crucial for obtaining the true absolute values of the stellar parameters (like the radii). Spectroscopic observations are more time consuming, and require much larger telescopes for targets of a given brightness. As pointed out by Paczyński (1997), one also needs accurate theoretical atmosphere models and/or calibrations to infer surface brightness on the basis of colours, line ratios or other observables.

The advantage is however that the error in the distance estimation is comparable to, or even smaller than, the dispersion of the PL -relation for Cepheids (Groenewegen 2005).

Nevertheless, eclipsing binaries (not only detached) have been recently used to determine precise distances on a different steps of the cosmic distance ladder, up to galaxies of the Local Group. Southworth et al. (2005), using various methods, calculated the distance to HD 23642 in the Pleiades cluster, confirming the inconsistency between the early *Hipparcos* results and other findings. Tens of binaries were analysed in the (e.g. Ribas 2004; Pietrzyński et al. 2013) and SMC (e.g. Hilditch et al. 2005; North et al. 2010). Finally, spectroscopy and radial velocities of several EBs in the Andromeda Galaxy (Ribas et al. 2005; Vilardell et al. 2010a,b) and M33 (Bonanos et al. 2006) were obtained, indicating the distance modulus fully compatible with other findings.

Despite all this effort and the potential behind the method, eclipsing binaries have never been used extensively to study the structure of the Milky Way, especially its inner parts. Ruciński has been discussing the application of

* Based on observations taken within the ESO VISTA Public Survey VVV, Programme ID 179.B-2002

† E-mail: xysiek@astro.puc.cl

W UMa binaries for this purpose (Ruciński 1997, 2004). The problem partially lays in the high and differential extinction towards the Galactic Center, which limits our magnitude range, and the crowding of the field. Another problem is a lack of a deep catalogue of EBs, coming from a long-cadence variability survey of the Milky Way. The deepest survey so far is OGLE (Udalski et al. 1992), but the only published catalogue with eclipsing binaries identified (Woźniak et al. 2002) comes from the OGLE-II phase where only selected fields of the Galactic Bulge were observed. EBs from this catalogue were analysed by Devor (2005), but without distance determination, and Groenewegen (2005) gave a list of EBs potentially useful for distance calculations, but again without the distances themselves.

Recently, two large infra-red galactic plane surveys started: the UKIRT Infrared Deep Sky Survey (UKIDSS; Lawrence et al. 2007), with its Galactic Plane Survey (GPS), and the VISTA Variables in the Via Lactea (VVV; Minniti et al. 2010). The latter observes the Bulge and disk area regularly, and the first data release is already published (DR1; Saito et al. 2012). The multi-epoch variability campaign in the K_S band will provide infra-red light curves for about 5×10^5 eclipsing binaries in the Bulge and disk, down to magnitude $K_S \sim 18$. This extensive and deep data set will thus be perfect to study the overall structure of the Galaxy, including its most inner and outer parts. The present paper is a first effort of this study, proving that our concept works using a relatively small sample. We present the selected sample of DEBs and their photometric data in Section 2. Sections 3 and 4 describe the method, and our initial results respectively. Finally in Section 5 we discuss the future possibilities and perspectives of this project.

2 SAMPLE AND NIR DATA

2.1 Initial target selection

Since the main variability campaign of the VVV survey is still not finished, we need to test our method on a well known sample of objects. We decided to use eclipsing binaries from the OGLE-II variable stars catalogue (Woźniak et al. 2002). Devor (2005) presented models of about 10000 of them obtained with the DEBiL code, and identified 3170 of them as “detached”. We selected this sample as our starting point. Groenewegen (2005) analysed the same catalogue by Woźniak et al. (2002) and found a similar number of targets, which he describes as “candidates for distance estimates”. We have done all the work independently of his catalogue.

Due to some limitations of the DEBiL code (see Section 3) we decided to pre-select only the “well” detached systems, defined as the ones for which a single eclipse occupies less than about 10 per cent of the whole orbital period. We got 625 objects, for which we recalculated and corrected the orbital periods, using a routine based on the analysis of variance (AoV) method (Schwarzenberg-Czerny 1989). The routine also provides the formally second best period, which sometimes occurred to be the true one. We also recalculated the DEBiL models (with 10000 iterations, see also Section 3), especially correcting the total observed I band magnitudes, which was originally given as the median value of all measurements, not the out-of-eclipse value. As the input to

the further steps we also used the given V band magnitude (in the OGLE system), which we treat as being out of the eclipse. This however must be taken with caution, since we have no warranty that the photometry has not been contaminated by an observation taken during an eclipse. By selecting only the “well” detached systems, we expect to lower the probability of such situation (i.e. less than 20 per cent of the systems would be contaminated).

2.2 NIR photometry from the VVV

The near infrared photometry comes from the merged Bulge JHK_S catalogue of point sources, prepared as a part of the DR1 of the VVV survey (Saito et al. 2012). The catalogue (v1.1) contains over 130 million sources from the Bulge area of the VVV survey ($-10 < l < 10$; $-10 < b < 5$), about 70 million of which are flagged as “stellar” in all bands. The photometric measurements were done by the Cambridge Astronomical Survey Unit (CASU). Fluxes were measured in several apertures of different sizes. For each target a single magnitude value is given. The catalogue has been generated by the VISTA Science Archive (VSA; Cross et al. 2012).

We have looked for the entries of the previously selected 625 targets in the merged JHK_S catalogue v1.1. We assumed a rather large tolerance in astrometry of 3 arcsec, i.e. we took only those VVV counterparts that were not further than 3 arcsec from the OGLE position in all three J , H and K_S bands. We found 506 matches for about 250 targets. Around half of the OGLE/DEBiL targets had a single match in the JHK_S catalogue, however in the most extreme cases up to 6 matches within the allowed area were found. Because we wanted our procedure to be as automated as possible, we did not do any additional inspection or rejections at this stage, and decided to rely on the further steps of the analysis and rejection criteria applied therein.

3 THE METHOD

This section describes the methods and steps we used in the analysis of the 625 DEBs, for which the initial light curve modeling was done, and later the 506 matches between OGLE and VVV.

3.1 Initial light curve modeling

The Detached Eclipsing Binary Light curve fitter (DEBiL fitter; Devor 2004, 2005) is a fully-automated computer program¹ which rapidly fits EB light curves to a simple EB model. Since its comparably fast and does not require any guidance from the user, the DEBiL fitter can systematically fit a large number of DEB light curves (LCs).

The DEBiL fitter assumes that the binary components are well detached (i.e. that the binary stars can be modeled as limb-darkened spheres with negligible refraction), and that 3rd light and dust reddening effects have been corrected. As

¹ The DEBiL source code and running examples are available on-line at: <http://www.cfa.harvard.edu/~jdevor/DEBiL.html>.

input, DEBiL requires a light curve, a period, and limb darkening coefficients; it then returns the best fit values and estimated uncertainties for the following eight parameters: orbital inclination (i), orbital eccentricity (e), epoch of periastron (t_0), argument of periastron (ω), fractional stellar radii (r_1, r_2), and the apparent stellar magnitude in the wavelength of the given LC (mag_1, mag_2). In addition to this, DEBiL provides the results of a suite of statistical tests, which quantify the quality of the fit.

DEBiL operates by first folding the LC by the given period, then removing outliers and smoothing the data to reduce its noise. The shape of the resulting phased LC is then measured to produce “initial guess” values for the above eight parameters, taking into account the shape distortion due to the smoothing. Next, DEBiL attempts to iteratively improve the model fit by running a large number of iterations, governed by the downhill simplex optimization method (Nelder & Mead 1965), in combination with simulated annealing (Kirkpatrick et al. 1983; Press et al. 1992), for improved reliability and robustness. In the final step, the best-solution is varied by small amounts, so to estimate the uncertainty of each of the resulting eight model parameters.

3.2 Binary component identification

The DEBiL fitter attempts to fit an essentially geometric model to the LC. More specifically, the DEBiL parameters only describe the relative sizes and the orbital orientation of the binary. To better understand the physics of the system, one needs to also find the stellar masses, ages, and chemical composition. This has traditionally been done through multi-epoch high-resolution spectroscopic observations. Unfortunately, such observations are comparably difficult to perform on large numbers targets, and can be prohibitive for very dim or hot stars. To this end we used the Method for Eclipsing Component Identification (MECI; Devor & Charbonneau 2006a,b), which fits a physical model to each DEB using only readily-available photometric data.

MECI is a fully-automated computer program² that is designed to work from the DEBiL model as a starting point, and further builds a physical model of the DEB. MECI assumes that the binarys stellar components formed together and evolved along their respective isochrones, without any mass transfer. As input, MECI requires a light curve, binary colors (optional but recommended), a period, the orbital parameters outputted by DEBiL, and assumed initial stellar compositions; it then returns the best fit values and estimated uncertainties for binary components masses and coeval age. It is also possible to give specific values of observed magnitude in different bands (with errors); MECI then returns the absolute magnitude, so the distance may be calculated directly from the difference between the two values.

MECI operates by iterating through triplets of primary-component mass, secondary-component mass, and age, and from each triplet deriving the expected stellar radii, luminosities, and colors of the binary components. It then uses these results to construct a model light curve and binary

colors, and compares them to the given observations. The triplet that produces the model that best matches the observed data is assumed to be the most likely solution. Finally, the triplet values are varied by small amounts, so to estimate the uncertainties of the measured masses and age. Since the given isochrone library contains a finite number of cases, it is inevitable that the best-fit triplet of some DEBs will be at the maximal or minimal mass or age available. In such cases MECI cannot give a bounded uncertainty estimate, but only an upper or lower limit on the physical properties of the binary.

3.3 Reddening-free indices and isochrones

One of the biggest problems in calculating distances with a non-geometrical method is the interstellar extinction and reddening. It is especially difficult in the direction to the galactic Bulge, not only because of large amount of dust we are looking through, but also due to crowding. Two stars separated by just few seconds of arc can be located several kiloparsecs from each other, which means completely different values of A_V or $E(B - V)$. The most popular extinction maps by Schlegel et al. (1998) do not have enough resolution and they need to be corrected in the area of the Bulge. Sumi (2004) was analysing the extinction in the OGLE-II fields, but he gave only average values of A_V and A_I for each field. More recently Gonzalez et al. (2011, 2012) provided a high-resolution reddening and metallicity map for the whole Bulge, but still the resolution is limited to $2' \times 2'$ pixels. Finally, three-dimensional extinction maps were published by Chen et al. (2013), but they do not cover the areas where our objects are located.

We decided to use the reddening-free indices, as in Catelan et al. (2011). They give a number of pseudo-magnitude quantities m , which are combinations of magnitudes in 3 bands in the form of:

$$m_X = M_1 - c(M_2 - M_3),$$

where $M_{1,2,3}$ are the magnitudes in given bands and c is a multiplication coefficient dependent on the extinction law assumed. The coefficient c is given in such way, that within a given extinction law, defined as ratios of extinction values in the given bands $A_1 : A_2 : A_3$, the following equation is true:

$$M_1 - c[M_2 - M_3] = (M_1 + A_1) - c[(M_2 + A_2) - (M_3 + A_3)].$$

Moreover it can be shown that if the absolute magnitudes are used to build the reddening-free indices, those indices $-M_X$ can be used to calculate distances (Catelan et al. 2011), i.e.:

$$(m_X - M_X) = 5(\log d - 1),$$

thus they seem to be perfectly suited for the purpose of our project.

When building the indices of the OGLE V, I and VVV J, H, K_S magnitudes, we assumed extinction ratios for each band as in Table 1, which follow a canonical extinction law of $R = 3.09$, the same as Catelan et al. (2011). The values of A_λ/A_V for OGLE filters are taken from Vanhollebeke et al. (2009), however they claim that those values are reproduced by $R = 2.4$. We repeated the procedure they follow (from Cardelli et al. 1989), and found that for given values of λ_{eff} ,

² The MECI source code and running examples are available online at: <http://www.cfa.harvard.edu/~jdevor/MECI.html>.

Table 1. Extinction law in the form of extinctions in each band relative to the extinction in Johnson’s V band – A_V .

Filter	λ_{eff}	A_λ/A_V	Ref.
V_{OGLE}	0.542	1.017	1
I_{OGLE}	0.871	0.506	1
J_{VVV}	1.254	0.280	2
H_{VVV}	1.646	0.184	2
$K_{S,VVV}$	2.149	0.118	2

Ref.: (1) Vanhollenbeke et al. (2009); (2) Catelan et al. (2011).

the extinction coefficients A_λ/A_V for OGLE filters are actually reproduced by $R = 3.09$. Thus our extinction law is consistent with the canonical one.

On this basis we defined five indices:

$$m_1 = I - 0.563(V - K_S) \quad (1)$$

$$m_2 = K_S - 0.231(V - I) \quad (2)$$

$$m_3 = H - 1.136(J - K_S) \quad (3)$$

$$m_4 = J - 0.722(I - K_S) \quad (4)$$

$$m_5 = K_S - 1.229(J - H), \quad (5)$$

which, except for m_3 , are obviously different than the ones used by Catelan et al. (2011). First, we used them to produce reddening-free isochrones for MECI. For this purpose we used two *Padova* sets (Girardi et al. 2000; Marigo et al. 2008), calculated for OGLE and VVV systems separately, and merged them into one set of a Y^2 format. We modified each isochrone in such a way that instead of $V - R$, $V - I$, $V - J$, $V - H$, $V - K$ we used $V - m_1 \dots V - m_5$ respectively. Then, for each target we calculated the five reddening-free indices on the basis of target’s out-of-eclipse magnitudes in the five bands (separately for each of the 506 matchings between VVV and OGLE). As the input for MECI we used four “pseudo-colours”: $m_1 - m_2$, $m_1 - m_3$, $m_1 - m_4$ and $m_1 - m_5$, as well as the five indices themselves (in this way only the reddening-free photometry was used by MECI) for calculating distance modules. It is worth to note that in case of the reddening-free photometry these are the distances more reliable, not the ones given directly by the code in the output file. For the final value of the distance we took a weighted average of the five values from different indices, and its error as a distance uncertainty.

This approach also has its disadvantages. The indices are combinations of three photometric measurements, each having its individual errors, which obviously propagate and accumulate in the errors of the indices themselves. As it is discussed in Catelan et al. (2011), also the use of the indices may narrow the range of colours (in mag units) leading for example to more difficulties in recognition of certain features on colour-magnitude diagrams. Moreover, as mentioned before, the values of multiplication coefficients depend on the extinction law assumed, which is not the standard one in the galactic Bulge. However, we still benefit from that approach because, as shown in further sections, in the direction to the Bulge we observe objects which are also in front of and behind it. Applying the values of A_V or $E(B - V)$ found for the Bulge to the objects located closer leads to further inconsistencies in the distance and absolute magnitudes obtained (Ratajczak et al. 2013). We do not know *a priori* where a given system resides, as it is actually the

goal of this research, and which extinction law should be the correct one, so we need a more universal approach to the extinction problem, and the reddening-free indices seem to be the best option. The choice of a particular law was of course arbitrary.

The choice of the grid of metal abundances Z was somewhat arbitrary as well. The selected values are 0.0001, 0.0004, 0.0007, 0.001, 0.004, 0.007, 0.01, 0.02, 0.03. The values below solar are similar to the ones available in the original Y^2 set, but supplemented with 0.007 and 0.0007 to better sample the metallicity space. The only value above solar – $Z = 0.03$ – was the upper limit of the *Padova* set in the time the analysis was done. The significant difference between Y^2 and *Padova* is that the *Padova* models used were evolved from the ZAMS, while Y^2 includes pre-main-sequence evolution. We could obviously benefit from using isochrones with wider range of available ages, but the *Padova* set may be calculated strictly for OGLE and VVV photometric systems, so no further transformations are required, thus the uncertainties are reduced.

3.4 Solution selection criteria

For all 506 input data sets (one set for each OGLE-VVV match) we run MECI nine times – one time for each set of isochrones of a given metallicity. From the solutions of a single run (one value of Z) MECI by itself selects the one with the smallest score. We then had to choose the value of metallicity, which provided the lowest-score solution for a given input set. From these solutions we filtered out only those which met the following criteria:

- the MECI score, which was derived by combining the reduced chi-square of the best-fit models LC and colors, was smaller than 3;
- all the fitted parameters were bounded (no upper or lower limits), and had uncertainties smaller than their values;
- the distance uncertainties were smaller than 5 per cent.

In this way we could select those solutions which seem to be more realistic and secure. The 5% relative error in distance corresponds to few hundreds of parsecs at 5-10 kpc – the vicinity of the galactic Bulge. This allows us to distinguish separate structures, like single arms. Otherwise the targets would be located along the line of sight more uniformly than we actually see it, single features would be undistinguishable, and the final results not conclusive. In vast majority of multiple OGLE-VVV matches we managed to select most likely the best one, since the others gave significantly higher scores (worse fit). Surprisingly, it was not always the one where the VVV coordinates were the closest to the OGLE ones. For several cases however an ambiguity remained.

After that filtering we ended up with about 100 solutions. This number is small enough to allow for a visual inspection of the model light curves and their comparison with observational data. We found a number of bad fits related to seemingly good models, and we rejected them. We could also solve the remaining ambiguities, and for each target select only *one* reliable model, or reject all if none was satisfactory.

The last selection step involved checking the consistency between the resulting distances and predictions based on the

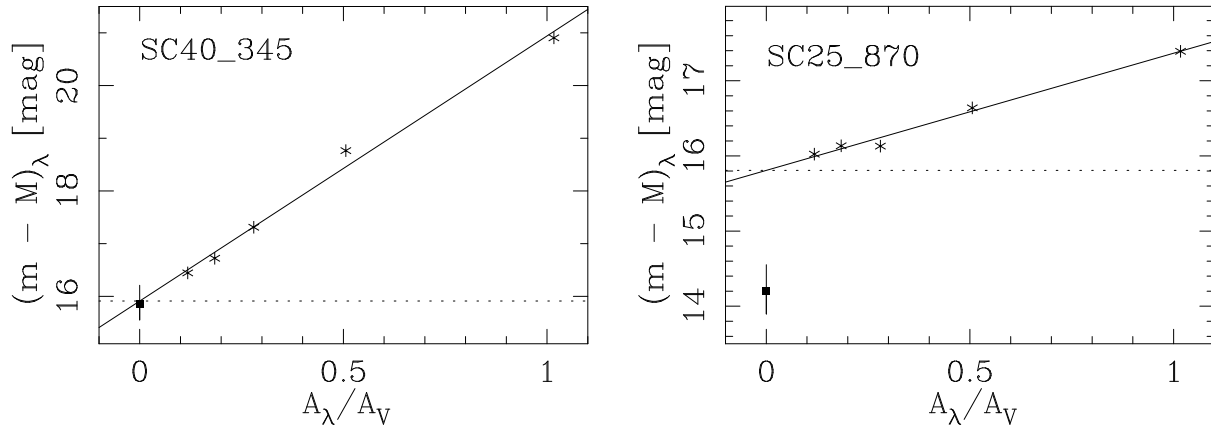


Figure 1. Examples of a solution approved (left) and rejected (right) in the last selection step. A_λ/A_V is the ratio of the extinction in a given band to the extinction in Johnson’s V , as in Table 1. Black squares mark the distance modules related to the distances calculated by MECI, and their error bars refer to the 15 per cent tolerance of those distances. Asterisks mark distance modules in bands (from left to right) K_S , H , J , I , and V predicted by the best-fitting isochrones. Solid line represents the linear fit to these modules. Its slope is the extinction in Johnson’s V band, and its intercept (marked with a dotted line) is the isochrone-predicted distance modulus in case of no extinction. If it is consistent with the calculated one, we approve such a solution.

best-fitting isochrones. For each remaining solution we generated two *Padova* isochrones (in OGLE and VVV systems) giving the best-fitting age and Z . Then we calculated the systems’ total absolute magnitudes in all five bands – M_λ , and after that the apparent distance modules – $(m - M)_\lambda$. We fitted a straight line on the A_λ/A_V vs. $(m - M)_\lambda$ plane, where the A_λ/A_V values were taken from the Tab. 1. In this approach, the slope of the line is simply the extinction coefficient in Johnson’s V band, and intercept with the $(m - M)$ axis is the distance modulus without extinction $(m - M)_0$. We then translated this modulus to a distance $(m - M)_0 = 5(\log d_0 - 1)$ and compared it to the distance obtained earlier in our fitting procedure. We rejected those solutions, for which the difference between two distances was larger than 15 per cent (3σ if σ is the largest error allowed). We believe that in this way we excluded systems with large systematic distance errors, and found reliable values of A_V for the remaining ones. The method is presented in Fig. 1. Approved (left) and rejected (right) cases are shown. After this step, we finally ended up with only 23 systems, which we present in the following Section. We list them in Table 2 together with their coordinates and photometric measurements. Their phase-folded I -band light curves and models are presented in the Appendix A.

4 RESULTS

4.1 Orbital and physical parameters

The output of the DEBiL and MECI codes is a set of orbital and physical parameters of each eclipsing system. Orbital parameters, namely the period, absolute major semi-axis, sine of the inclination, eccentricity and argument of the periastron (if $e > 0$), are summarised in Table 3. If the value of e was smaller than its formal error (18 cases), we show it as zero, however it was never held fixed during any fitting. One can see that all the orbits may be truly circular, especially considering short orbital periods. For at least two of the five eccentric systems the resulting eccentricity is not

much bigger than its uncertainty, and all five have their ω indifferent from $90/270^\circ$ – a case when phases of the two eclipses differ by 0.5, as for a circular orbit. All of the light curves, presented in Fig. A1, seem to show such a situation.

Other parameters, like masses, radii, ages, and metallicities (of the best-fitting isochrone), are given in Table 4. In the Figure 2 we plot the components of every system on the mass-radius plane, together with the best-fitting isochrone. It is worth noting that the radii in Tab. 4 come from the fractional ones – r_1, r_2 – calculated by DEBiL, and the major semi-axis calculated with the 3rd Keplerian law on the basis of the known period and masses found by MECI. These are not radii taken directly from the isochrones, so the match between the models and our results may serve as an independent test for the correctness of our analysis.

One can see, that the precision in determination of stellar parameters is not very high. The typical error is of the order of 20-30 per cent and reaches less than 5 per cent just for few single cases. Nevertheless, in most cases our parameters within errors match the models quite nicely, also when the two components lay far one from another (like for SC11_1200 or SC40_345). In two systems – SC17_41 and SC12_3218 – the match was initially very bad, probably due to a well-known issue that geometric light-curve-fitting codes, like the DEBiL, suffer from. In case of partially-eclipsing systems the ratio of the radii r_2/r_1 is poorly constrained, and very often degenerized with its multiplicative inverse value r_1/r_2 . In the same time this should not have influenced MECI, as it uses the observed brightness of the whole system, which has not much to do with the fraction of the radii. After inverting the radii, the data fit much better to the isochrones. Similar situation might have occurred in some other systems, like SC27_662 or SC42_4279, but the errors in masses and radii are too large to confirm that.

At this stage (with current data) we can not use our results for detailed study of the stellar structure and evolution but we are able to point out potentially interesting systems which deserve more attention and detailed analysis, including radial velocity measurements and direct determi-

Table 2. Summary data for the 23 resulting systems. DEBiL ID, coordinates (α , δ from OGLE, and galactic l, b), VVV tile number, and OGLE-II and VVV photometry are given.

DEBiL ID	α	δ	l [$^\circ$]	b [$^\circ$]	Tile no.	V_{OGLE} [mag]	I_{OGLE} [mag]	J_{VVV} [mag]	H_{VVV} [mag]	$K_{S,VVV}$ [mag]
SC3_2344	17:53:26.95	-30:08:25.5	-0.1580	-2.0797	305	17.14 \pm 0.12	15.79 \pm 0.02	14.92 \pm 0.04	14.49 \pm 0.05	14.32 \pm 0.06
SC10_863	18:19:51.37	-22:31:24.3	9.3825	-3.5399	298	18.86 \pm 0.11	16.97 \pm 0.05	15.78 \pm 0.02	15.32 \pm 0.03	15.15 \pm 0.04
SC11_853	18:20:45.98	-22:30:33.7	9.4936	-3.7190	284	18.17 \pm 0.05	16.54 \pm 0.07	15.42 \pm 0.02	14.97 \pm 0.02	14.81 \pm 0.03
SC11_1200	18:20:54.22	-22:21:50.4	9.6372	-3.6791	284	17.49 \pm 0.11	16.02 \pm 0.02	15.51 \pm 0.02	15.18 \pm 0.02	15.07 \pm 0.04
SC11_1274	18:21:14.62	-22:19:49.6	9.7038	-3.7329	284	19.90 \pm 0.12	17.91 \pm 0.09	16.76 \pm 0.05	16.17 \pm 0.06	16.16 \pm 0.09
SC12_1664	18:16:26.54	-24:00:08.6	7.7054	-3.5442	297	19.56 \pm 0.11	17.41 \pm 0.19	16.63 \pm 0.07	16.28 \pm 0.10	16.25 \pm 0.13
SC12_3218	18:16:01.45	-23:33:21.2	8.0541	-3.2488	297	18.76 \pm 0.18	15.83 \pm 0.13	14.43 \pm 0.01	13.75 \pm 0.01	13.53 \pm 0.01
SC15_2498	17:47:44.01	-22:59:00.2	5.3379	2.6811	365	19.32 \pm 0.13	17.39 \pm 0.02	16.19 \pm 0.07	15.69 \pm 0.08	15.54 \pm 0.09
SC16_2053	18:10:01.41	-26:21:58.3	4.9302	-3.3936	295	18.69 \pm 0.11	16.99 \pm 0.20	15.78 \pm 0.04	15.37 \pm 0.05	15.23 \pm 0.07
SC17_41	18:11:11.42	-26:40:19.6	4.7866	-3.7694	281	17.52 \pm 0.06	16.23 \pm 0.02	15.49 \pm 0.03	15.22 \pm 0.04	15.09 \pm 0.05
SC18_3886	18:07:16.43	-27:03:16.8	4.0295	-3.1878	294	16.27 \pm 0.03	15.12 \pm 0.01	14.20 \pm 0.02	13.88 \pm 0.02	13.80 \pm 0.02
SC18_4766	18:07:09.52	-26:56:00.5	4.1232	-3.1067	294	19.88 \pm 0.15	18.21 \pm 0.02	17.15 \pm 0.19	16.95 \pm 0.27	16.81 \pm 0.29
SC18_5161	18:06:47.19	-26:51:15.6	4.1522	-2.9957	294	17.46 \pm 0.05	16.13 \pm 0.02	15.20 \pm 0.03	14.85 \pm 0.04	14.67 \pm 0.05
SC22_2938	17:56:28.02	-30:47:05.7	-0.3876	-2.9661	291	18.53 \pm 0.06	16.70 \pm 0.15	15.27 \pm 0.04	14.68 \pm 0.04	14.47 \pm 0.05
SC22_4501	17:56:29.58	-30:31:49.9	-0.1643	-2.8436	291	18.15 \pm 0.06	15.93 \pm 0.02	14.46 \pm 0.02	13.93 \pm 0.02	13.67 \pm 0.02
SC23_784	17:57:35.48	-31:30:55.8	-0.9013	-3.5393	291	17.17 \pm 0.09	15.47 \pm 0.01	14.25 \pm 0.02	13.86 \pm 0.02	13.69 \pm 0.02
SC23_1648	17:58:10.94	-31:19:43.8	-0.6762	-3.5558	291	19.54 \pm 0.13	17.24 \pm 0.13	15.92 \pm 0.08	15.43 \pm 0.08	15.22 \pm 0.09
SC27_662	17:48:29.79	-35:26:43.1	-5.2595	-3.8882	274	16.96 \pm 0.06	15.46 \pm 0.02	14.50 \pm 0.01	14.07 \pm 0.02	13.99 \pm 0.02
SC40_345	17:50:51.05	-33:38:16.8	-3.4546	-3.3814	289	17.77 \pm 0.09	16.00 \pm 0.03	14.88 \pm 0.02	14.41 \pm 0.03	14.23 \pm 0.03
SC41_2400	17:52:23.10	-33:01:55.7	-2.7688	-3.3496	289	17.81 \pm 0.15	15.95 \pm 0.13	15.19 \pm 0.03	14.74 \pm 0.04	14.58 \pm 0.04
SC42_4161	18:08:47.24	-26:26:27.9	4.7310	-3.1871	295	17.90 \pm 0.05	16.27 \pm 0.06	15.38 \pm 0.03	14.97 \pm 0.04	14.85 \pm 0.05
SC42_4279	18:09:21.47	-26:25:51.9	4.8014	-3.2941	295	18.24 \pm 0.11	16.32 \pm 0.04	15.13 \pm 0.02	14.68 \pm 0.03	14.50 \pm 0.03
SC45_1450	18:03:30.49	-29:55:13.2	1.1177	-3.8589	278	18.43 \pm 0.11	17.23 \pm 0.05	16.41 \pm 0.08	16.03 \pm 0.10	15.94 \pm 0.12

Table 3. Orbital parameters of the researched systems.

DEBiL ID	P [d]	a [R_\odot]	$\sin i$	e	ω [$^\circ$]
SC3_2344	2.526650	18.593 \pm 1.198	0.9989 \pm 0.0013	0.0	—
SC10_863	3.471626	34.956 \pm 3.601	0.9956 \pm 0.0046	0.004 \pm 0.003	44.14 \pm 376.80
SC11_853	3.746524	32.859 \pm 5.666	0.9885 \pm 0.0044	0.0	—
SC11_1200	4.445230	22.492 \pm 0.483	0.9997 \pm 0.0017	0.0	—
SC11_1274	1.708079	8.198 \pm 0.143	1.0000 \pm 0.0047	0.0	—
SC12_1664	2.812648	10.852 \pm 0.143	0.9960 \pm 0.0057	0.0	—
SC12_3218	2.306802	22.031 \pm 1.241	0.9888 \pm 0.0150	0.140 \pm 0.017	90.83 \pm 94.25
SC15_2498	2.937350	28.648 \pm 2.444	0.9987 \pm 0.0067	0.040 \pm 0.010	275.44 \pm 104.24
SC16_2053	3.394874	30.748 \pm 5.602	0.9963 \pm 0.0045	0.0	—
SC17_41	4.280280	27.828 \pm 1.535	0.9970 \pm 0.0060	0.0	—
SC18_3886	2.427420	20.656 \pm 2.081	0.9944 \pm 0.0044	0.123 \pm 0.028	269.96 \pm 88.82
SC18_4766	4.873240	16.826 \pm 0.288	1.0000 \pm 0.0048	0.0	—
SC18_5161	2.459740	9.520 \pm 0.255	0.9806 \pm 0.0052	0.0	—
SC22_2938	4.996538	40.658 \pm 3.305	0.9957 \pm 0.0128	0.222 \pm 0.200	87.34 \pm 104.22
SC22_4501	2.715658	26.007 \pm 2.346	0.9845 \pm 0.0038	0.0	—
SC23_784	3.619210	24.043 \pm 0.374	1.0000 \pm 0.0013	0.0	—
SC23_1648	5.277104	44.126 \pm 3.529	0.9995 \pm 0.0035	0.0	—
SC27_662	2.485568	22.205 \pm 1.622	0.9887 \pm 0.0027	0.0	—
SC40_345	2.873292	24.896 \pm 0.826	0.9990 \pm 0.0025	0.0	—
SC41_2400	2.361774	10.427 \pm 0.426	0.9998 \pm 0.0010	0.0	—
SC42_4161	3.483948	26.199 \pm 0.882	0.9999 \pm 0.0138	0.0	—
SC42_4279	3.290610	28.497 \pm 2.032	0.9874 \pm 0.0037	0.0	—
SC45_1450	1.845630	18.264 \pm 1.998	0.9884 \pm 0.0079	0.0	—

nation of stellar parameters. There is for example a couple of systems with one or both components evolving out of the main sequence. Interesting examples are SC12_1664 and SC18_5161 where both components are solar analogs, most likely being already sub-giants.

From Tab. 4 and Fig. 2 we see that the majority of the systems contain massive ($M > 10 M_\odot$) and young ($t < 10$ Myr) O and B type stars, sometimes after the main sequence evolution stage. Only few older F and G type stars can be found. In general, the most metal-abundant stars can

be found among the least-massive ones, but on the other hand, the objects with the smallest Z can be found uniformly spread along the mass range. It is nevertheless clear that high masses, young ages and metal depletion tend to be preferred in our solutions.

It is not very surprising in case of masses and ages. Massive, short-living stars have high intrinsic brightnesses, so can be visible from very large distances. One has to remember that the OGLE-II sample is significantly limited in magnitude range and area on the sky, so it is expected that

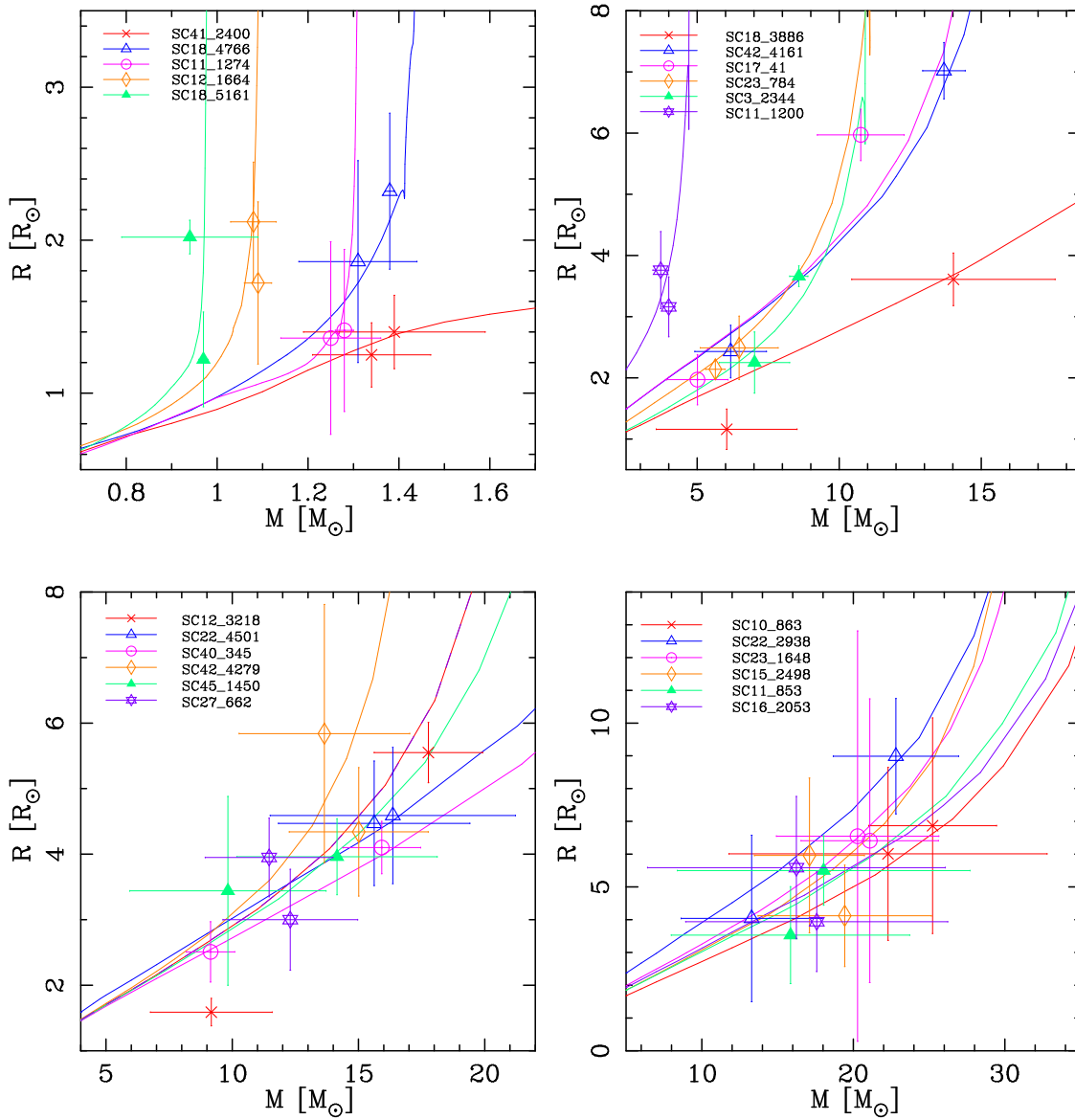


Figure 2. Mass-radius diagram for the 23 described systems. Each system’s components and the best-fitting isochrone are plotted in the same colour. On the lower left pannel the isochrones for SC12_3218 and SC27_662 are the same. Colour figure available in the on-line version of the manuscript.

the further in distance we go, the higher fraction young and massive stars will pose. Also the magnitude range of the VVV survey has its limitations. In the same time we do not expect to see many systems composed of bright, evolved, late-type giants. They are usually found in long-period binaries, and among the 3170 systems classified as detached in the DEBiL catalogue, there are only about 60 (< 2 per cent) systems with $P > 10$ d. This is consistent with 0 systems in the final sample counting 23 targets. Such late type giants will be very bright in the infrared, so many of them may be saturated in K_S and thus not included in the catalogues. Fig. 2 shows that our objects are only main sequence stars and sub-giants.

The low values of Z are however a bit surprising, because recent stellar formation is thought to occur in metal-enriched environments. The tendency of finding metal-poor

solutions may thus be a problem of our method or the selection of the metallicity grid. We noticed a general weak dependency of the solution’s score (and resulting stellar parameters) on the Z of the isochrone, which for example makes it difficult to estimate the realistic uncertainty in Z , but in case of the metal-poorest solutions ($Z = 0.0001$) we clearly see that they are the formally-best ones. However, due to this weak dependency, we do not claim that the given values of Z are the true ones, rather that are indicating more or less significant metal depletion or enrichment of a given system, especially taking into account the age-metallicity degeneration on the main sequence. This is an issue which will be more carefully investigated in the future, because the recent sample of systems is too small. However, metal abundances in various areas of the Milky Way and surroundings (the membership of the systems to a certain

Table 4. Stellar parameters of the researched systems. Ages and metal abundances refer to the best-fitting isochrones.

DEBiL ID	M_1 [M_\odot]	M_2 [M_\odot]	R_1 [R_\odot]	R_2 [R_\odot]	t [Gyr]	Z
SC3_2344	6.48±1.37	7.02±1.24	2.49±0.52	2.25±0.50	0.023±0.014	0.0001
SC10_863	25.23±4.22	22.29±10.47	6.87±3.29	6.01±2.64	0.005±0.004	0.0001
SC11_853	18.04±9.66	15.85±7.87	5.50±1.06	3.53±1.48	0.005±0.004	0.0004
SC11_1200	3.72±0.28	4.00±0.22	3.76±0.63	3.16±0.49	0.118±0.045	0.0300
SC11_1274	1.28±0.02	1.25±0.11	1.41±0.53	1.36±0.63	2.28±1.39	0.0004
SC12_1664	1.08±0.05	1.09±0.03	2.12±0.39	1.72±0.53	7.47±3.39	0.0100
SC12_3218	9.17±2.41	17.77±2.15	1.59 ^a ±0.21	5.55 ^a ±0.46	0.009±0.004	0.0001
SC15_2498	17.10±3.63	19.43±5.72	5.96±2.36	4.12±1.55	0.006±0.004	0.0004
SC16_2053	16.24±9.83	17.58±8.65	5.59±2.17	3.94±1.52	0.005±0.004	0.0007
SC17_41	5.01±1.08	10.76±1.53	1.97 ^a ±0.41	5.07 ^a ±0.42	0.013±0.004	0.0040
SC18_3886	14.02±3.58	6.04±2.48	3.61±0.43	1.16±0.33	0.006±0.004	0.0001
SC18_4766	1.38±0.01	1.31±0.13	2.32±0.51	1.86±0.66	2.64±1.31	0.0070
SC18_5161	0.94±0.15	0.97±0.01	2.02±0.11	1.22±0.31	6.25±2.08	0.0001
SC22_2938	22.81±4.14	13.29±4.66	8.99±1.76	4.04±2.54	0.005±0.003	0.0070
SC22_4501	16.36±4.86	15.62±3.79	4.59±1.04	4.47±0.95	0.005±0.002	0.0004
SC23_784	8.58±0.32	5.64±0.34	3.66±0.17	2.14±0.15	0.023±0.003	0.0007
SC23_1648	20.28±5.36	21.08±4.53	6.55±6.26	6.41±4.33	0.006±0.002	0.0010
SC27_662	11.46±2.53	12.30±2.67	3.95±0.60	3.00±0.77	0.009±0.004	0.0001
SC40_345	15.92±1.54	9.14±0.96	4.10±0.40	2.51±0.46	0.005±0.001	0.0001
SC41_2400	1.39±0.20	1.34±0.13	1.40±0.24	1.25±0.21	0.008±0.001	0.0200
SC42_4161	13.69±0.75	6.18±1.26	7.02±0.46	2.43±0.43	0.012±0.004	0.0040
SC42_4279	13.65±3.38	15.01±2.75	5.84±1.97	4.34±0.98	0.012±0.007	0.0001
SC45_1450	14.15±3.97	9.83±3.89	3.96±0.58	3.44±1.44	0.008±0.007	0.0001

Notes: ^a radii were inverted

Galaxy structures will be discussed in the next Section) are not well measured, or the spread is relatively large.

4.2 Distances and the structure of the Galaxy

Calculating the distances for a sufficient number of stars and finding the overall structure of the Galaxy were the main goals of this research. We ended up with only 23 from over 3000 initial DEB's from the starting DEBiL catalogue, but it is enough to mark several major features of the Milky Way and show the overall usefulness of our method. The distance, extinction in Johnson's V band, and the putative membership of a given system to a certain structure are given in Table 5.

The distance and the celestial coordinates can be easily transformed to a position in galactic coordinates (X, Y, Z). In this representation the Sun is in (0, 0, 0), and following Churchwell et al. (2009) we assume that the Galactic Center is in (8.0 kpc, 0, 0). Positions of our 23 systems in the galactic plane (X, Y) are presented in Fig. 3. To find their membership, we compared them to the reconstruction by Churchwell et al. (2009). See also Fig. B1.

Except for SC15_2498, all the systems are seen around the galactic latitude $b \sim -3^\circ$, so the further from the Sun we go, the lower under the disk we look – about 800 pc at $X \sim 14$ kpc (six systems in far Perseus and Norma arms), and almost 3 kpc for the furthest objects. This is of course due to the selection of fields from the OGLE-II survey. This obviously has its implications on studying the structure behind the Bulge, and may explain the low metallicities. Tracing the arms and thickness of the disk in this area will be more accurate with targets visible closer to the galactic equator.

The positions of the closest 13 binaries match very well the positions of spiral arms and the galactic Bulge. It is especially interesting in the far (behind the Bulge) part of the Perseus Arm ($d \sim 13$ -14 kpc), where we put 5 systems, and for which the arm's curvature can be found. Three more systems are found behind the edge of the stellar disk found by Minniti et al. (2011) at 13.9 ± 0.5 kpc from the Center, in a distance where the reconstruction by Churchwell et al. (2009) shows a weak, far extension of the Sagittarius arm. Their eventual membership to this arm is however uncertain because of the large distance from the galactic plane: from 1.36 to 1.7 kpc. Notice also that there are no systems found in a very strong Scutum-Centaurus arm behind the Bulge, about 20 kpc from the Sun. At the latitude of $b \sim -3^\circ$ any targets at this distance would be about 1 kpc below the galactic plane.

There is a number of systems found even further, on distances corresponding to the Sagittarius dwarf spheroidal galaxy (Sgr dSph) and its stream. If confirmed, they would be the first eclipsing binaries found in this galaxy. Among them one can find the most massive stars of our sample. Six of the objects classified as possible members of Sgr dSph can be found on the lower right panel of the Fig. 2. Two others are SC45_1450 and SC42_4161. The latter, together with SC22_2938, are the only two from that sub-sample that have their parameter errors small enough not to overlap on the mass-radius diagram. Yet, both have the isochrones nicely matching the data points. SC42_4161 is also relatively bright and its components are on a significantly different stages of evolution. Its spectroscopic follow up should be possible to do.

The low number of systems found in front of the Bulge – just two – is not very surprising. Due to the magnitude

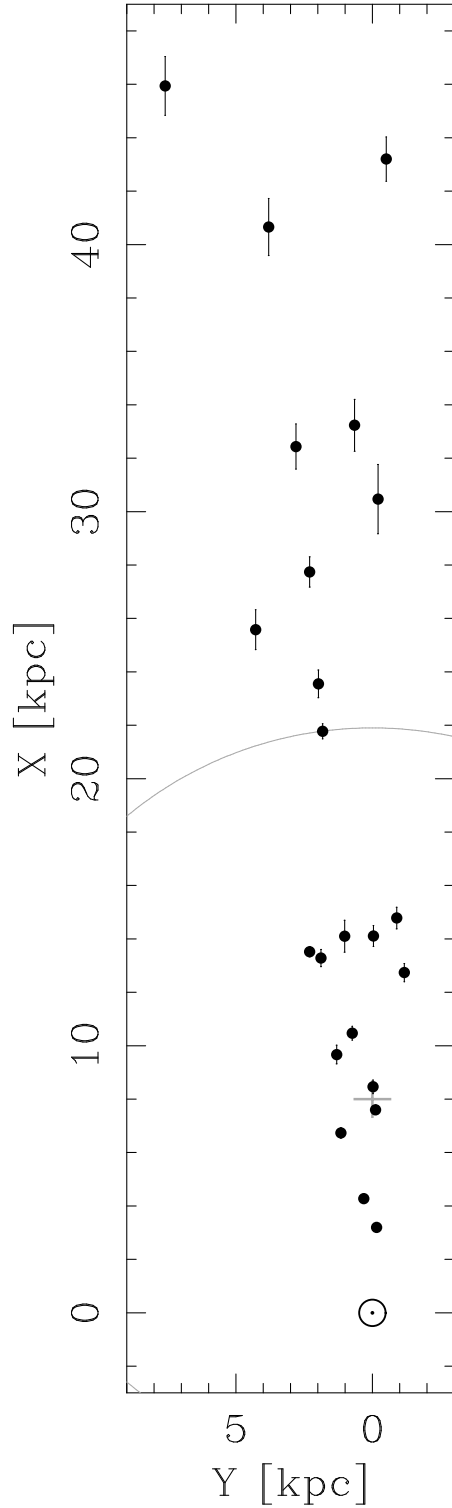


Figure 3. Positions of the 23 researched systems in the galactic plane. The Sun is marked at (0,0) with the traditional symbol, and the Galactic Center at (8.0, 0) with the grey cross. The grey solid line indicates an approximate edge of the Galaxy’s stellar disk as traced by clump giants (Minniti et al. 2011). The separation between the arms and the Bulge is clearly seen. Most of the systems are seen behind the Bulge, some of them may be related to the Sgr dSph galaxy.

Table 5. Distances, V-band extinctions and putative membership of the researched systems.

DEBiL ID	d [kpc]	A_V [mag]	Belongs to...
SC3_2344	8.46 ± 0.26	4.029	<i>Bulge</i>
SC10_863	46.65 ± 1.10	5.247	<i>Sgr dSph?</i>
SC11_853	26.00 ± 0.75	4.846	<i>Sag[f]/Sgr dSph?</i>
SC11_1200	13.74 ± 0.19	3.054	Per[f]
SC11_1274	6.84 ± 0.20	4.127	<i>Bulge</i>
SC12_1664	9.78 ± 0.35	1.461	Far/ <i>Bulge</i>
SC12_3218	13.44 ± 0.32	6.908	Per[f]
SC15_2498	40.88 ± 1.10	5.320	<i>Sgr dSph?</i>
SC16_2053	32.61 ± 0.85	4.968	<i>Sgr dSph?</i>
SC17_41	21.90 ± 0.28	3.613	ScC[f]/Sag[f]?
SC18_3886	10.51 ± 0.27	3.855	Far/ <i>Bulge</i>
SC18_4766	14.16 ± 0.59	2.461	Per[f]/Nor[f]
SC18_5161	4.29 ± 0.04	2.367	Nor[n]
SC22_2938	30.51 ± 1.30	5.618	<i>Sgr dSph?</i>
SC22_4501	14.12 ± 0.39	6.092	Per[f]/Nor[f]
SC23_784	7.61 ± 0.18	4.804	<i>Bulge</i>
SC23_1648	43.29 ± 0.83	5.904	<i>Sgr dSph?</i>
SC27_662	12.82 ± 0.34	4.421	Per[f]
SC40_345	14.83 ± 0.40	5.029	Nor[f]
SC41_2400	3.21 ± 0.02	2.475	ScC[n]
SC42_4161	27.88 ± 0.56	4.381	<i>Sgr dSph?</i>
SC42_4279	23.67 ± 0.52	5.259	Sag[f]?
SC45_1450	33.31 ± 0.97	3.851	<i>Sgr dSph?</i>

Note: Structures not being a part of the galactic disk are marked with italics. The abbreviations of galactic spiral arms are as follows: Far – Far 3kpc Arm; Nor – Norma Arm; Per – Perseus Arm; Sag – Sagittarius Arm; ScC – Scutum-Centaurus Arm. [f] means the far (behind the Bulge) and [n] near part of the arm. *Sgr dSph?* means the Sagittarius dwarf galaxy; the membership is uncertain because of actually unknown structure of this galaxy and its streams. Question marks related to Sag[f] in 3 cases are due to a significant distance from the galactic plane (1.36-1.7 kpc).

limitations and reduced volume sample, only a small fraction of all the systems contain late type stars. In our case it’s only 5 of all 23. The two closest systems – SC18_5161 and SC41_2400 – contain F and G stars and are significantly brighter than the other three: SC11_1274, SC12_1664 and SC18_4766 ($V > 19.5$ mag), located in the Bulge and behind it. The combination of VVV and OGLE data thus appears to be suited much better for the poor-studied far areas of the Galaxy than for the closer ones.

4.3 Ages and metallicities

Among the various output parameters of the codes, one can also find the age and metal content of the system. As was explained previously, the age is calculated directly by MECI within a set of isochrones of a given Z , while the value of Z was found by looking for a lowest score among various MECI solutions. Such an approach, at least in principle, allows us to trace the age and metallicity distribution in the Milky Way. Unfortunately, the current sample of 23 is too small to derive any conclusions, especially considering the metal-depletion tendency mentioned in Sect. 4.1.

In Figure 4 we present the same spatial distribution of our systems as in Fig. 3 but with age and metallicity color-coded. The age t is given in Gyr and the metal abundance

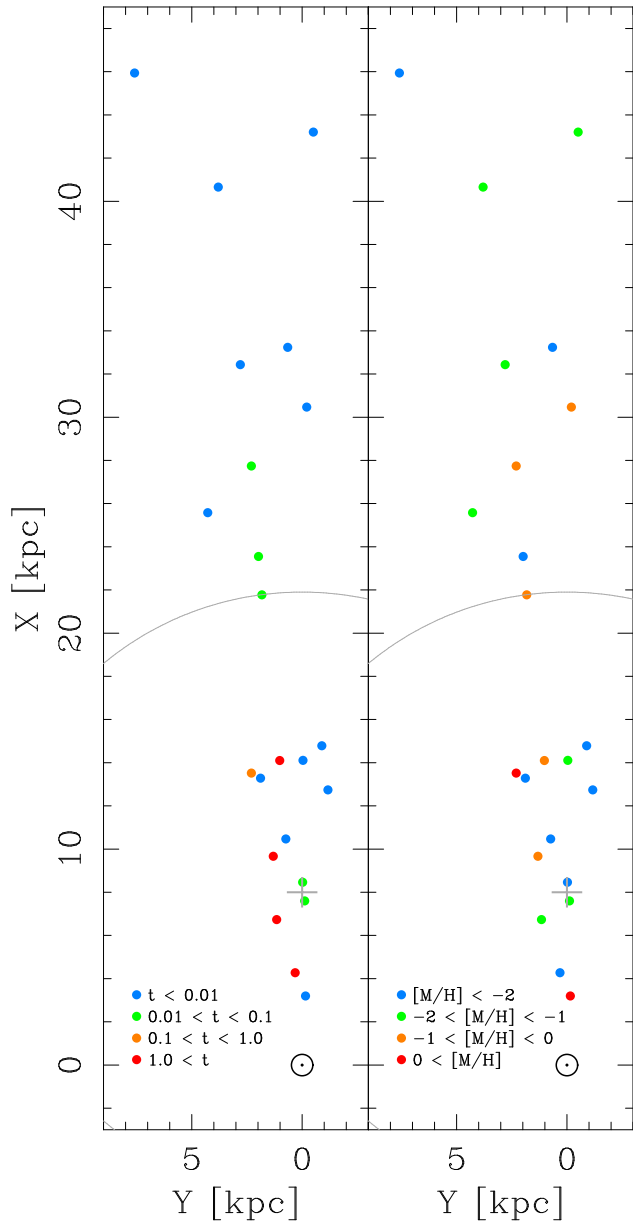


Figure 4. Ages (left) and metallicities (right) of the researched systems in the same spatial representation as in Fig. 3. The age is given in Gyr and the metal abundance Z is translated into $[M/H] = \log(Z/0.019)$. The Galactic Center and the approximate edge of the stellar disk are also shown. Colour figure is available in the on-line version of the manuscript.

Z is translated into $[M/H] = \log(Z/0.019)$. The data does not show any significant trends. The oldest systems are seen in arms as well as in the Bulge. They are not seen outside the Galaxy, but this may be explained by the observational limitations mentioned before. The ages of the most massive stars are found to be of several millions of years. This means that there may still exist gas and dust related to the star formation regions. In case of the Sgr dSph, scenarios of recent star formations are possible, and the traces of interstellar gas have been found (e.g. Monai et al. 2005, and references therein), but for the galactic systems, it is surprising to see the recent star formation so far from the galactic disk. The

metallicities are distributed more-less uniformly, regardless the location, also within the same spiral arm. It is noticeable, that the Sgr dSph member candidates show quite a large spread of metallicities – from $[M/H] \simeq -2.3$ to -0.4 , but as it was mentioned, the values of Z in our case are not well constrained.

4.4 Sources of uncertainties and incorrect solutions

There are various factors which negatively affect our analysis, either increasing the errors or causing that a given solution is rejected. First one is the possibility of having a photometric measurement in the V, J, H or K_S band done during an eclipse. Due to the pre-selection of “well-detached” systems only, the probability of such a situation is smaller than 20 per cent, but we deal with measurements in four filters. If even only one is affected, the resulting pseudo-colours and reddening-free indices will be incorrect, so will be the formally best solution. This may make many solutions to be rejected in any stage of the selection process.

Another factor, which may have the same consequences, is the inaccuracy of period determination. It is a well known issue that in cases of eclipses of similar depth the period-finding algorithm finds one which is two times shorter than the true one. On the other hand, for systems having one of the two eclipses very shallow, the period found is twice as long as the true one. In our sample we found by eye examples of both situations and corrected them, but obviously it is not the purpose when one is creating a pipeline, which should be able to work on tens of thousands of light curves. Moreover, the periods found may be incorrect at the fourth or fifth decimal number. In such cases the model obtained is less accurate than for a true period. We also found several such cases, but we suppose that many have been omitted and analyzed with inaccurate period. We however expect that this had not as big influence on the final results as the previous or the next factor.

The Bulge is obviously a very crowded area, so one can expect that the light curves will be at some level contaminated by a light of a background star. In case of eclipsing binaries the “third light” changes the observed colours and makes the eclipses shallower. Looking at our light curves in Fig. A1, one can find cases of eclipses at the level of only 0.1-0.2 mag. While many “contaminated” solutions were probably rejected due to the high score value or large error in distance, some of them might have been recognised as acceptable. Unfortunately, the fitting for the third light is very difficult in case of single-band light curves, and was not implemented in DEBiL, nor in MECI.

Another possible source of uncertainties is the usage of one extinction law for all the systems. It is already a known fact that towards the Bulge the reddening law is non-standard and non-uniform (Nataf et al. 2012, and references therein). Despite the reddening-free coefficients solve the problem of extinction and reddening in a very elegant way, they still depend directly on the extinction law assumed. Considering that, the usage of one set of coefficients to the whole analysis is an obvious simplification, and has an influence on the main goal of this study – distance determination. Unfortunately, we can’t rely on the recent published extinction maps (Gonzalez et al. 2012; Nataf et al.

2012; Chen et al. 2013), because within one line of sight we may deal with stars located in front of, inside and behind the Bulge in the same time, and the reddening and extinction should be different for each of them. To be treated correctly, the extinction should be calculated for each target separately, which is not implemented in the procedure.

As we mentioned before, the *Padova* evolutionary tracks we used start at the ZAMS. This means that we will have no solutions for pre-main-sequence (PMS) systems, or systems containing one PMS component and the other evolving on the main sequence already. For such objects MECI gives only upper or lower limits of the physical parameters, and such solutions are being rejected. It is also possible that a local score minimum have been found in the accepted range of parameters, while the global one would be far outside, and the value of score at the edge of the parameter space was still higher than in the local minimum. Such a solution would still be accepted. This could at least partially explain the observed tendency to find young and metal-poor solutions, i.e. young systems far from the galactic disk.

Another explanation of this may be an effect of the warped and/or flared disk of the Milky Way, as it was used to explain the observed overdensities of stars in various regions of the Galaxy. For further reading on this topic we refer to López-Corredoira et al. (2012), where a short summary and numerous references are presented in Section 1. We also find possible a scenario that some of the presumably young binaries were rejected from their parent clusters in a process of dynamical interactions, and should have large velocities (Fujii & Portegies Zwart 2012). This can be easily verified with spectroscopic observations.

Finally, in our analysis we also used only one limb darkening (LD) table, prepared for the solar chemical composition (Kurucz 1992; Claret 1998, 2000). In general, the usage of improper LD coefficients affects such parameters like fractional radii or inclination. However, the precision and, what is probably more important, the sampling of the available light curves is usually not enough to be fragile for subtle changes in the LD coefficients. In most cases we have less than 30 points per eclipse and for magnitudes $I > 17$ the spread reaches 0.1 mag. Thus we believe that the analysis of most of the systems was not affected by this issue, however we can't exclude that in case of the brightest systems.

5 PROSPECTS FOR THE FUTURE

The final number of accepted models (23) is only a small fraction of the initial number of systems (3170). It is not only due to the fact that many solutions were rejected. In the future many improvements can be done, so that we will have hundreds or thousands of systems located uniformly in the field of the Bulge and disk, and the structure of the Galaxy will be traced more effectively. At this stage we mainly suffer from the inhomogeneity of the target distribution in the sky. We rely on the OGLE-II fields, concentrated around certain galactic latitudes. At larger distances we look below the disk, which makes the study of the structure of the arms difficult. OGLE-III covers a much larger area in the direction to the Bulge, but the catalogue of eclipsing binaries has not been published yet. This will be solved once the variability campaign of the VVV project is finished. VVV

maps uniformly the whole galactic Bulge ($-10 < l < +10$, $-10 < b < +5$) and the disk ($295 < l < 350$, $-2 < b < +2$). The variability campaign assumes 80 epochs in K_S for the whole area, down to magnitude 18, and 5×10^5 eclipsing binaries are expected to be found. The photometric information also includes measurements in two more filters than we use now – Z, Y .

The matching between the OGLE-II and VVV catalogues was relatively poor. Notice, that the VVV counterpart was found for less than 1/3 of the DEBs, and for about half of them the matching was ambiguous. VVV itself should thus provide data sufficient to effectively trace the structure of the spiral arms, especially behind the Bulge. On the other hand, combination of light curves in K_S from the VVV and in I from the OGLE-III (once the catalog is published), and other photometric informations, will allow for very precise study of the overlapping regions. The structures in front, inside and behind the Bulge (including the Sgr dSph) should then be well analysed.

Our work should benefit not only from increasing the number of targets and photometric data, but also some changes in the procedures applied. Firstly, we will extend the range of ages and chemical compositions of the isochrones we use. This will allow us to say something not only about the distribution of stars, but also about ages and abundance gradients across the Galaxy.

Changes also can be made to the fitting procedures. At the current stage DEBiL assumes spherical stars. Adding the possibility of working on tidally-distorted objects will surely be very profitable. Only 20 per cent of the whole sample of DEBs was classified as "well detached", and with ~ 80 points per light curve in the VVV variability campaign we can rather expect to find short-period DEBs with wide eclipses and prominent ellipsoidal variations.

Finally, since our approach depends on the law we assume, we expect that the results would change with different extinction and reddening laws, based on different values of R . It is possible that the solutions we've found are simply the ones following the law we assumed. The desirable solution would be to fit for extinction and reddening individually for each target, or implement one (probably complicated) extinction law, suitable for any location in the Galaxy.

6 SUMMARY AND CONCLUSION

We presented models and parameters of 23 detached eclipsing binaries (DEBs) with OGLE light curves and VVV photometric measurements. Using the concept of reddening-free indices (Catelan et al. 2011) we calculated distances to the systems and have been able to match their location with major structures of the Milky Way. With the strict criteria applied we believe to have only the most reliable results. We conclude that our approach is suitable for tracing the structure of the Galaxy with DEBs identified in the VVV, OGLE and also UKIDS/GPS surveys. The magnitude range of the VVV data seem to be perfect for tracing the structure of spiral arms behind the Bulge, and possibly identifying the first DEBs in the Sagittarius dwarf spheroidal galaxy and the associated Sagittarius stream. In principle, also the age, metallicity and extinction distributions can be found, but this requires many more objects than our initial sample

contains and an uniform coverage of the Bulge area. This may be achieved once the variability campaign of the VVV survey is finished.

ACKNOWLEDGMENTS

We would like to thank the anonymous Referee for valuable comments, which helped us to improve this work.

We gratefully acknowledge use of data from the ESO Public Survey programme ID 179.B-2002 taken with the VISTA telescope, and data products from the Cambridge Astronomical Survey Unit (CASU). We acknowledge the support from the Basal Center for Astrophysics and Associated Technologies CATA PFB-06, and by the Ministry for the Economy, Development, and Tourism's Programa Iniciativa Científica Milenio through grant P07-021-F, awarded to The Milky Way Millennium Nucleus. K.G.H. acknowledges support provided by the Proyecto FONDECYT Postdoctoral No. 3120153. We also acknowledge the support provided by the Polish National Science Center through grants 2011/03/N/ST9/01819, 5813/B/H03/2011/40 and 2011/03/N/ST9/03192.

REFERENCES

- Bonanos A. Z. et al., 2006, *ApJ*, 652, 313
 Cardelli J. A., Clayton G. C., Mathis J. S., 1989, *ApJ*, 345, 245
 Catelan M. et al., 2011, in McWilliam A., ed., *RR Lyrae Stars, Metal-Poor Stars, and the Galaxy*, Carnegie Obs. Astrophys. Ser., 5, 145
 Claret A., 1998, *A&A*, 335, 647
 Claret A., 2000, *A&A*, 363, 1081
 Chen B. Q., Schultheis M., Jiang B. W., Gonzalez, O. A., Robin A. C., Rejkuba M., Minniti D., 2013, *A&A*, 550, A42
 Churchwell E. et al., 2009, *PASP*, 121, 213
 Cross N. J. G. et al., 2012, *A&A*, 548, 119
 Devor J., 2004, *American Astronomical Society Meeting Abstracts*, 205
 Devor J., 2005, *ApJ*, 628, 411
 Devor J., Charbonneau D., 2006, *Ap&SS*, 304, 351
 Devor J., Charbonneau D., 2006, *ApJ*, 653, 648
 Devor J., Charbonneau D., O'Donovan F. T., Mandushev G., Torres G., 2008, *AJ*, 135, 850
 Fujii M. S., Portegies Zwart S., 2012, *Science*, 334, 1380
 Girardi L., Bressan A., Bertelli G., Chiosi C., 2000, *A&AS*, 141, 371
 Gonzalez O. A., Rejkuba M., Zoccali M., Valenti E., Minniti D., 2011, *A&A*, 534, A3
 Gonzalez O. A., Rejkuba M., Zoccali M., Valenti E., Minniti D., Schultheis M., Tobar R., Chen B., 2012, *A&A*, 543, A13
 Groenewegen M. A. T., 2005, *A&A*, 439, 559
 Hilditch R. W., Howarth I. D., Harries T. J., 2005, *MNRAS*, 357, 304
 Kirkpatrick S., Gelatt C. D., Vecchi M. P., 1983, *Science*, 220, 671
 Kurucz R. L., 1992, in Barbuy B., Renzini A., eds, *Proc. IAU Symp. 149, The Stellar Populations of Galaxies*. Kluwer, Dordrecht, p. 225
 Lawrence A. et al., 2007, *MNRAS*, 379, 1599
 López-Corredoira M., Moitinh A., Zaggia S., Momany Y., Carraro G., Hammersley P. L., Cabrera-Lavers A., Vázquez R. A., 2012, arXiv:1207.2749 [astro-ph.GA]
 Marigo P., Girardi L., Bressan A., Groenewegen M. A. T., Silva L., Granato G. L., 2008, *A&A*, 482, 883
 Minniti D. et al., 2010, *NewA*, 15, 433
 Minniti D., Saito R. K., Alonso-García J., Lucas P. W., Hempel M., 2011, *ApJL*, 733, L43
 Monai S., Bonifacio P., Sbordone L., 2005, *A&A*, 433, 241
 Nataf D. M. et al., 2012, arXiv:1208.1263 [astro-ph.GA]
 Nelder J. A., Mead R., 1965, *Computer Journal*, 7, 308
 North P., Gauderon R., Barblan F., Royer F., 2010, *A&A*, 520, A74
 Paczyński B., 1997, in M. Livio, ed., *Conference Paper Space Telescope Science Institute Series, The Extragalactic Distance Scale*, Cambridge Univ. Press, Cambridge, p. 273
 Pietrzyński G. et al., 2013, *Nat*, 495, 76
 Press W. H., Teukolsky S. A., Vetterling W. T., Flannery B. P., 1992, *Numerical Recipes in C. The Art of Scientific Computing*, Cambridge Univ. Press, Cambridge
 Ratajczak M., et al. 2013, in preparation
 Ribas I., 2004, *NewAR*, 48, 731
 Ribas I., Jordi C., Vilardell F., Fitzpatrick E. L., Hilditch R. W., Guinan E. F., 2005, *ApJ*, 635, L37
 Ruciński S. M., 1997, *AJ*, 113, 407
 Ruciński S. M., 2004, *NewAR*, 13, 458
 Saito R. K. et al., 2012, *A&A*, 537, 107
 Schlegel D. J., Finkbeiner D. P., Davis M., 1998, *ApJ*, 500, 525
 Schwarzenberg-Czerny, A., 1989, *MNRAS*, 241, 153
 Southworth J. W., Maxted P. F. L., Smalley B., 2005, *A&A*, 429, 645
 Sumi T., 2004, *MNRAS*, 349, 193
 Udalski A., Szymański M., Kałużny J., Kubiak M., Mateo M., 1992, *AcA*, 42, 253
 Vanhollebeke E., Groenewegen M. A. T., Girardi L., 2009, *A&A*, 498, 95
 Vilardell F., Ribas I., Jordi C., Fitzpatrick E. L., Guinan E. F., 2010a, *A&A*, 509, A70
 Vilardell F., Ribas I., Jordi C., Fitzpatrick E. L., Guinan E. F., Tsodikovich Y., Mazeh T., 2010b, in Prša A., Zejda M., eds, *Binaries – Key to Comprehension of the Universe*, Astronomical Society of Pacific, San Francisco, p. 375
 Woźniak P. R. et al., 2002, *AcA*, 52, 129

APPENDIX A: LIGHT CURVES

Phase-folded *I*-band light curves of the 23 researched systems. Dots show single magnitude measurements and gray lines are the best-fitting models found by MECI. Because the solutions are done for a general case of non-zero eccentricity, the zero-phase is set to the time of periastron. As it is discussed, most likely all systems have circular orbits.

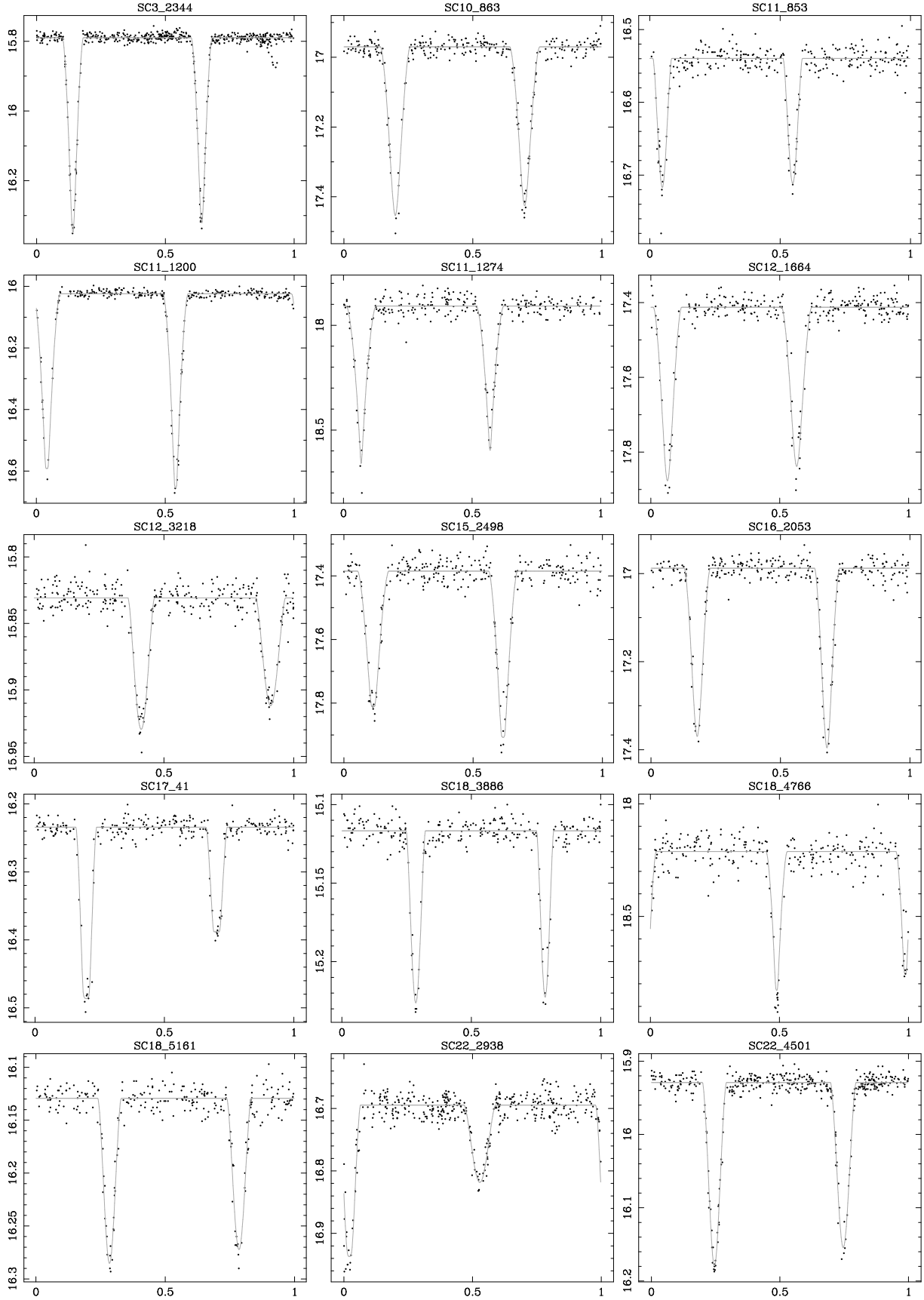


Figure A1. OGLE *I*-band light curves (dots) and MECI models (lines) for the researched systems.

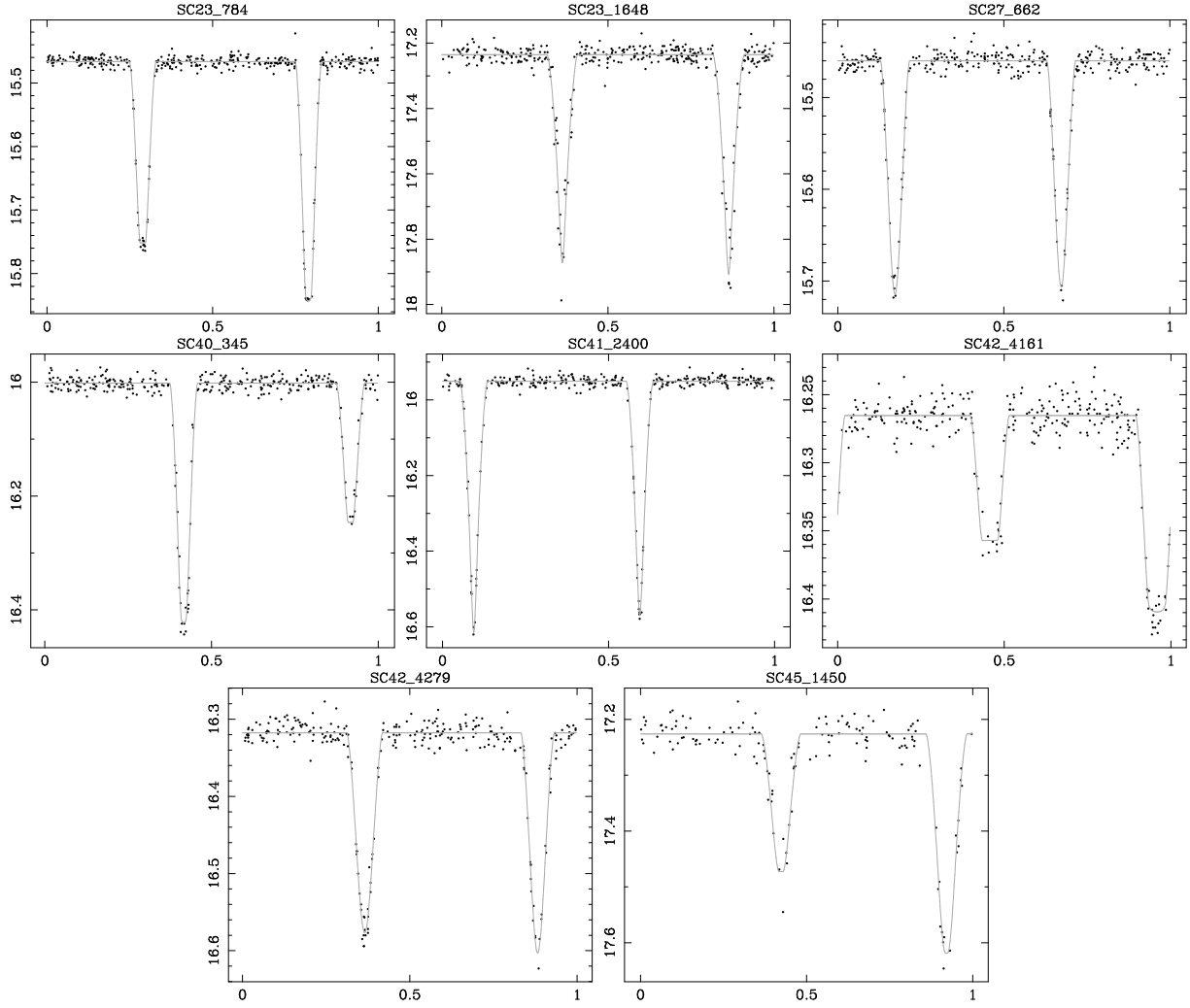


Figure A2. Continuation of Figure A1.

APPENDIX B: RECONSTRUCTION OF THE MILKY WAY

The 16 closest systems from our sample plotted over the reconstructed image of the Milky Way from Churchwell et al. (2009).

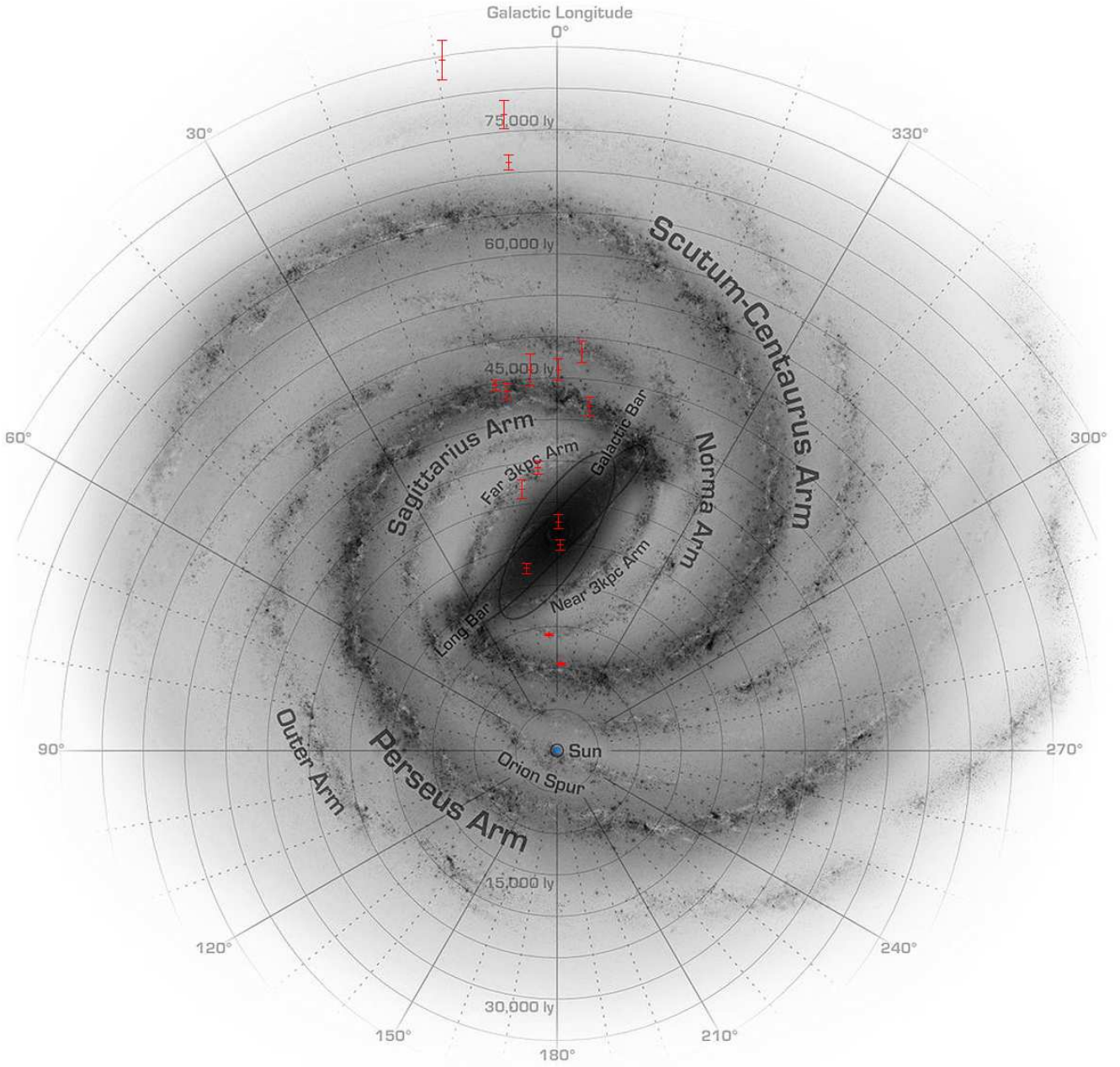


Figure B1. The sixteen closest eclipsing binaries from the 23 researched plotted over the reconstruction of the Milky Way from Churchwell et al. (2009). Colour figure is available in the on-line version of the manuscript.